X-ray Absorption Spectroscopy To Probe Surface Composition and Surface Deprotection in Photoresist Films

Joseph L. Lenhart,*,† Daniel A. Fischer,‡ Sharadha Sambasivan,‡ Eric K. Lin,*,‡ Ronald L. Jones,‡ Christopher L. Soles,‡ Wen-li Wu,‡ Dario L. Goldfarb,§ and Marie Angelopoulos§

Sandia National Laboratories, P.O. Box 5800, MS 0888, Albuquerque, New Mexico 87185, National Institute of Standards and Technology, 100 Bureau Drive, Gaithersburg, Maryland 20899, and IBM, T. J. Watson Research Center, Yorktown Heights, New York 10598

Received November 18, 2004. In Final Form: February 4, 2005

Near-edge X-ray absorption fine structure spectroscopy (NEXAFS) is utilized to provide insight into surface chemical effects in model photoresist films. First, NEXAFS was used to examine the resist/air interface including surface segregation of a photoacid generator (PAG) and the extent of surface deprotection in the film. The concentration of PAG at the resist−air interface was higher than the bulk concentration, which led to a faster deprotection rate at that interface. Second, a NEXAFS depth profiling technique was utilized to probe for compositional gradients in model resist line edge regions. In the model line edge region, the surface composition profile for the developed line edge was dependent on the post exposure bake time.

1. Introduction

Photolithography is the primary patterning tool used by integrated circuit (IC) chip manufacturers to print circuit tree patterns on wafers and accounts for about 35% of the manufacturing cost of today's IC chip. As IC chip feature sizes shrink, it becomes critical to control the shape, size, and roughness in the lithographic patterns. For example, when patterning on the 100 nm size scale, the pattern dimension and roughness must be controlled to less than 10 nm, a length scale approaching the molecular size of the polymer molecules composing the resist films.[1]

To understand the impact of interfacial phenomena on lithographic patterns, it is important to understand the general patterning process. General papers about photolithography are available.[2−6] Several basic steps are present as illustrated by the schematic in Figure 1. In step 1, a photoresist polymer film is spun cast onto the substrate. The film is heated (post-apply baked, PAB) to remove residual solvent. After the PAB, a UV exposure pattern is generated in the photoresist film. While industrial photoresist may contain several additives, one critical additive is a photoacid generator (PAG). Upon UV exposure, the PAG in the resist film decomposes, generating an acid product. An example of a PAG[7] is shown in

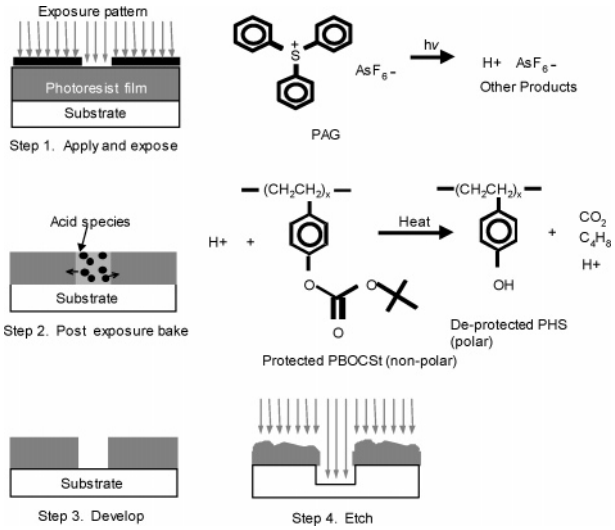

Figure 1. A schematic of the photolithography process.

Figure 1. In step 2, the exposed photoresist is baked again, called a post-exposure bake (PEB). During PEB, the acid diffuses in the resist film and catalyzes a chemical reaction in the polymer, which changes the polymer solubility in a developer solution. Step 3 involves removing the soluble portion of the polymer film in the developer, leaving a pattern in the resist film. In step 4, the pattern is transferred to the underlying substrate via a reactive ion etch, where the resist film provides etch resistance.

The solubility switch in the photoresist during PEB can be caused by two different mechanisms. In a negative tone resist, the exposed region of the film becomes less soluble in developer, usually due to an acid-catalyzed curing reaction in the film. In a positive tone resist, the exposed region is more soluble in the developer. For positive tone resists, the solubility switch is caused by an acid-catalyzed deprotection reaction in the polymer. An example of a typical positive tone resist deprotection

* Corresponding authors. E-mail: jllenha@sandia.gov. E-mail: eric.lin@nist.gov.
† Sandia National Laboratories.
‡ National Institute of Standards and Technology.
§ IBM.

(1) National Technology Roadmap for Semiconductors; The Semiconductor Industry Association: San Jose, CA, 2001.
(2) Ito, H. *IBM J. Res. Dev.* **1997**, *41*, 69.
(3) Wallraff, G. M.; Hinsberg, W. D. *Chem. Rev.* **1999**, *99*, 1801.
(4) Reichmanis, E.; Houlihan, F. M.; Nalamasu, O.; Neenan, T. X. *Chem. Mater.* **1991**, *3*, 394.
(5) Hinsberg, W. D.; Houle, F. A.; Sanchez, M. I.; Wallraff, G. M. *IBM J. Res. Dev.* **2001**, *45*, 667.
(6) Reichmanis, E.; Nalamasu, O.; Houlihan, F. M. *Acc. Chem. Res.* **1999**, *32*, 659.
(7) Uhrich, K. E.; Reichmanis, E.; Baiocchi, F. A. *Chem. Mater.* **1994**, *6*, 295.

10.1021/la047160z CCC: $30.25
Published on Web 03/31/2005

reaction is shown in Figure 1, step 2, where a nonpolar *tert*-butyl protective group on poly(*tert*-butyloxy-carbonyloxy-styrene) (PBOCSt) is cleaved from the backbone polymer, converting it to a polar polyhydroxystyrene (PHS).

Many factors can impact the size, shape, and roughness of the developed pattern in the photoresist film, including segregation of the photoacid generator (PAG) molecules or other resist additives,[7] diffusion of the photogenerated acid at the interface between the exposed and unexposed regions of the film,[8] outgassing of photoresist materials during the deprotection reaction,[9] film thickness effects,[10] and the photoresist composition and extent of deprotection at the interface between exposed and unexposed areas.[11] In addition, the pattern shape, size, and roughness are sensitive to processing parameters such as bake temperature, bake time, UV exposure dose, etc.[3]

With shrinking pattern sizes, photolithography will become increasingly prone to surface phenomena, which can degrade the developed pattern. A striking example of these interfacial effects in chemically amplified resist is the degradation in the lithographic performance due to airborne contamination. Trace levels of airborne amines can induce a thin, insoluble skin on the resist surface leading to deviation in the lithographic pattern called t-topping or closure.[12−17] Air purification systems, and the application of a protective overcoat on the resist film, have been used to prevent surface contamination of the resist by the airborne amine, eliminating the t-topping phenomena.[12,14] Another example of an interfacial problem that can become important with decreasing feature sizes is roughness in a developed lithographic pattern (line edge roughness or LER). While LER can be caused by optical effects, such as image projection,[18] material factors such as photogenerated acid diffusion, resist deprotection at the interface between the exposed and unexposed regions of the film,[19−22] resist chemistry,[11] and dissolution behavior[23] can also contribute to LER.

Due to the complex interfacial problems that can impact the shape, size, and roughness in lithographic patterning, it is important to develop and utilize new tools to probe the interfacial composition and structure of photoresist films. Here, we demonstrate the utility of NEXAFS for providing information about lithographic interfaces. First, focus is placed on the surface composition and surface deprotection at the air interface in a model resist film. Second, a NEXAFS technique is described to extract surface composition profiles in a model line edge region, offering the potential to provide detailed chemical information about compositional gradients in lithographic patterns.

2. Experimental Section[24]

2.1. Materials and Methods. The model resist solution was composed of 0.7 g of protected polymer poly(*tert*-butyloxy-carbonyloxy-styrene, $M_{n,r} = 15\,000$) (PBOCSt) mixed with 0.035 g of the photo acid generator, bis(*p-tert*-butylphenyl) iodonium perfluoro-octane-sulfonate (PFOS) (0.05 mass fraction relative to the polymer). This mixture was dissolved in 20 mL of propylene glycol methyl ether acetate (PGMEA). The resist solution was spun cast onto silicon wafers at 1500 rpm for 60 s and then post-apply baked (PAB) for 60 s at 100 °C. The PBOCSt/PFOS films were blanket exposed to ultraviolet radiation from a broadband source with wavelengths ranging between 220 and 260 nm with a total dose of 500 mJ/cm^2. After exposure, the films were post-exposure baked (PEB) at 100 °C for varying lengths of time. Polyhydroxystyrene, $M_{n,r} = 5000$, (PHS)/PFOS and polystyrene, $M_{n,r} = 24\,000$, (PS)/PFOS films were made according to the same procedures described above.

2.2. Near-Edge X-ray Absorption Fine Structure (NEXAFS) Spectroscopy. NEXAFS measurements were conducted at the U7A beamline of the National Synchrotron Light Source at Brookhaven National Laboratory. A monochromator with 600 line/mm grating, providing ±0.15 eV resolution, was used for all NEXAFS experiments. The monochromator energy scale was calibrated by the carbon K-edge π^* transition of graphite at 285.35 eV. All of the spectra were recorded at room temperature in the NIST − Dow material characterization chamber[25] at 10^{-6} Pa. The spectra were normalized to the incident beam intensity, I_0, by collecting the total electron yield intensity from a gold-coated 90% transmitting grid placed in the incoming X-ray beam path. The carbon fluorescence-yield intensity was measured utilizing a differentially pumped, UHV compatible proportional counter filled with 0.27 MPa of P-90 (90% methane, 10% argon) in an energy dispersive mode[26] to reduce background fluorescence from other elements. Surface-sensitive partial electron yield measurements were made (probe depth of approximately 1−6 nm) by applying a negative bias on the entrance grid of the channeltron electron detector. For the carbon K-edge spectra (260−330 eV), the electron yield detector was set with a negative bias of 150 eV. The spectra were collected with the incident beam at the magic angle (54.7°) relative to the sample to remove any polarization dependence. For the NEXAFS spectra in this paper, the experimental standard uncertainty in the peak position is similar to the grating resolution of ±0.15 eV. The relative uncertainty in the NEXAFS intensity is less than ±5% and was determined by multiple scans on a sample.

For some experiments, bilayer samples of PBOCSt and PHS were spun cast onto silicon wafers. The bottom PBOCSt layer was spun cast from solution with PGMEA and soft baked for 60 s at 130 °C. A top layer of PHS (with a 5% mass fraction of PFOS) was spun cast on PBOCSt from a solution of *n*-butanol. The samples were exposed to UV radiation and post-exposure baked for various times at 90 °C. After PEB, the soluble top portion of the bilayer film was removed (developed) by immersion in aqueous 0.26 N tetra-methylammonium-hydroxide solution. NEXAFS measurements were then conducted on the developed bilayer

(8) Fedynyshyn, T. H.; Thackeray, J. W.; Georger, J. H.; Denison, M. D. *J. Vac. Sci. Technol., B* **1994**, *12*, 3888.
(9) Dentinger, P. M. *J. Vac. Sci. Technol., B* **2000**, *18*, 3364.
(10) Fryer, D. S.; Nealey, P. F.; de Pablo, J. J. *J. Vac. Sci. Technol., B* **2000**, *18*, 3376.
(11) Lin, Q.; Sooriyakumaran, R.; Huang, W.-S. *Proc. SPIE* **2000**, *3999*, 230.
(12) Ito, H. *Jpn. J. Appl. Phys.* **1992**, *31*, 4273.
(13) Kozawa, T.; Uesaka, M.; Yoshida, Y.; Tagawa, S. *Jpn. J. Appl. Phys.* **1993**, *32*, 6049.
(14) Nalamasu, O.; Reichmanis, E.; Hanson, J. E.; Kanga, R. S.; Heimbrook, L. A.; Emerson, A. B.; Baiocchi, F. A.; Vaidya, S. *Polym. Eng. Sci.* **1992**, *32*, 1565.
(15) MacDonald, S. A.; Hinsberg, W. D.; Wendt, R.; Dlecak, N. J.; Willson, G. C.; Snyder, C. D. *Chem. Mater.* **1993**, *5*, 348.
(16) Hinsberg, W. D.; MacDonald, S. A.; Dlecak, N. J.; Snyder, C. D. *Chem. Mater.* **1994**, *6*, 481.
(17) Yoshino, H.; Itani, T.; Hashimoto, S.; Yamana, M.; Samoto, N.; Dasama, K.; Timko, A. G.; Nalamasu, O. *Microelectron. Eng.* **1997**, *35*, 153.
(18) Reynolds, G. W.; Taylor, J. W. *J. Vac. Sci. Technol., B* **1999**, *17*, 334.
(19) Patsis, G. P.; Glezos, N.; Raptis, I.; Valamontes, E. S. *J. Vac. Sci. Technol., B* **1999**, *17*, 3369.
(20) Schmid, G. M.; Smith, M. D.; Mack, C. A.; Singh, V. K.; Burns, S. D.; Willson, C. G. *Proc. SPIE* **2000**, *3999*, 675.
(21) Kim, Y.-S.; Kim, Y.-H.; Lee, S. H.; Yim, Y.-G.; Kim, D. G.; Kim, J.-H. *Proc. SPIE* **2002**, *4690*, 829.
(22) Yoshizawa, M.; Moriya, S. *J. Vac. Sci. Technol., B* **2002**, *20*, 1342.
(23) Flanagin, L. W.; Singh, V. K.; Willson, C. G. *J. Vac. Sci. Technol., B* **1999**, *17*, 1371.

(24) Certain commercial equipment, instruments, or materials are identified in this paper to specify the experimental procedure adequately. Such identification is not intended to imply recommendation or endorsement by the National Institute of Standards and Technology, nor is it intended to imply that the materials or equipment are necessarily the best available for the purpose.

(25) For detailed information about the NIST/Dow Soft X-ray Materials Characterization Facility at NSLS BNL, see: http://nslsweb.nsls.bnl.gov/nsls/pubs/newsletters/pdfs/96-nov.pdf

(26) Fischer, D. A.; Colbert, J.; Gland, J. L. *Rev. Sci. Instrum.* **1989**, *60*, 1596.

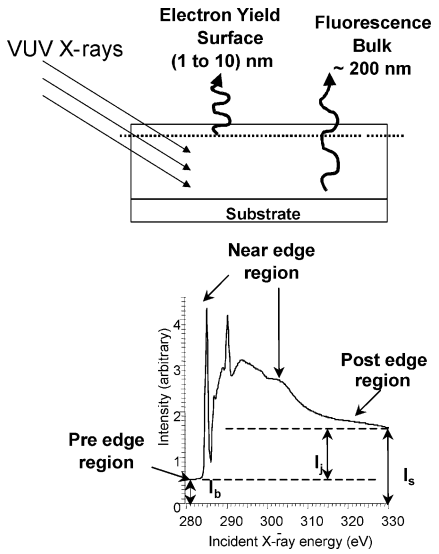

Figure 2. A schematic of the NEXAFS experiment and typical spectra.

samples as a function of the electron yield detector bias. For the depth profiling measurements on the bilayer surfaces, the negative bias on the electron yield detector was varied between 50 and 245 eV.

3. NEXAFS

Figure 2 shows a schematic depicting the principles of NEXAFS. The sample is exposed to tunable, polarized, monochromatic X-ray radiation from a synchrotron light source. In these experiments, the incident radiation is scanned over the carbon K-edge region, an energy range from 260 to 330 eV. X-rays are preferentially absorbed by the sample when the incident radiation is at the appropriate energy to allow the excitation of a core shell electron to an unoccupied molecular orbital. During electronic relaxation, Auger electrons and characteristic fluorescence photons are released. However, the electron yield signal in NEXAFS is comprised of both Auger electrons and inelastic electrons. The electronic relaxation processes may release more than one electron. These electrons can only escape from the top surface of the sample (1−10 nm). The fluorescence photons are detected from as deep as 200 nm within the sample. NEXAFS has elemental sensitivity because the characteristic binding energies (carbon, nitrogen, oxygen, and fluorine core electrons) are well separated in energy. In addition, due to the well-defined energy gap associated with a core shell/unoccupied orbital transition, NEXAFS is also sensitive to the bonding characteristics of the atom.[27]

Figure 2 also shows a carbon edge electron yield NEXAFS spectrum for PBOCSt. In the pre-edge region, the incident radiation is weakly absorbed by the sample. The intensity in this region, I_b, is the background signal (often from the substrate and sample, lower energy absorption edges, orbital transitions other than core level transitions, etc.). Above the carbon K edge (285 eV), the signal intensity (electron or fluorescence yield) increases when the incident radiation is strongly adsorbed by the sample. In the near-edge region, the peaks represent chemical bonding structure in the sample because the emission signal increases when the incident energy is the appropriate energy to cause an electron transition from the core 1s orbital to an unoccupied molecular orbital.

(27) Stöhr, J. *NEXAFS Spectroscopy*; Springer Series in Surface Science; Springer: Heidelberg, 1992; Vol. 25.

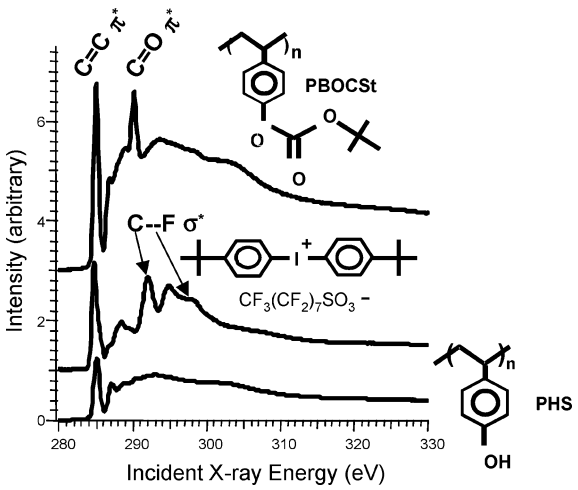

Figure 3. The electron yield NEXAFS spectra (offset for clarity) are shown for the pure resist components. The top spectrum is for PBOCSt. The middle is for PFOS. The bottom is for PHS.

The absorption edge represents the ionization of the core shell electron to the continuum. The edge jump, I_j, is defined as $I_s - I_b$. In the post-edge region, the signal intensity, I_j, represents the total amount of carbon (because the scan is over the carbon K-edge energy range) in the sampling volume. All of the NEXAFS spectra in this paper are pre-edge jump normalized to zero, by subtracting I_b from the spectrum. The well-defined peaks in the near-edge region of Figure 2 are a consequence of two factors: (a) the well-defined energy gap associated with the core level to unoccupied orbital transition, and (b) the synchrotron light source, which has high-intensity incident radiation that can be filtered to a monochromatic excitation source, allowing high resolution of the chemical peaks.

4. Results and Discussion

4.1. The Resist/Air Interface. Figure 3 shows the carbon edge NEXAFS spectra for the neat components used in our model resist system. The top spectrum is for the protected polymer, PBOCSt. The peak at 285.0 eV reflects the π^* transition [C 1s → $\pi^*_{C=C}$] associated with the carbon−carbon double bonds in the styrene ring. At 290.3 eV is a peak associated with the protective group, specifically the π^* transition [C 1s → $\pi^*_{C=O}$] of the carbon−oxygen double bond from the carbonyl group. The middle spectrum, for the PFOS PAG, also displays a sharp carbon−carbon π^* transition [C 1s → $\pi^*_{C=C}$] similar to PBOCSt. However, the broad peaks between 292.0 and 298.0 eV are due to σ^* transitions for carbon−fluorine bonds [C 1s → σ^*_{C-F}] at 292.0 and 298.0 eV and carbon−carbon bonds [C 1s → σ^*_{C-C}] at 295.0 eV on PFOS. The bottom spectrum is for the deprotected polymer, PHS, which also contains the strong π^* transition at 285.0 eV. Distinct peaks can be used to detect the individual resist components. For example, the peak at 290.3 eV in PBOCSt, associated with the protective group, is not present in PHS or PFOS, allowing the direct monitoring of the deprotection reaction. Also, the carbon−fluorine peaks in PFOS are not present in the other two spectra, although they may partially overlap with the carbon−carbon σ^* transition. Because the spectra are measured over the carbon K-edge, the peaks in Figure 3 represent core level transitions from the C 1s orbital to the unoccupied orbital.

Figure 4 shows the electron yield spectrum for the carbon K-edge of a PBOCSt/PFOS sample with PFOS mass fraction of 0.05. The carbon−fluorine σ^* peaks [C 1s → σ^*_{C-F}] (at 292.0 and 298.0 eV) from the PFOS are clearly

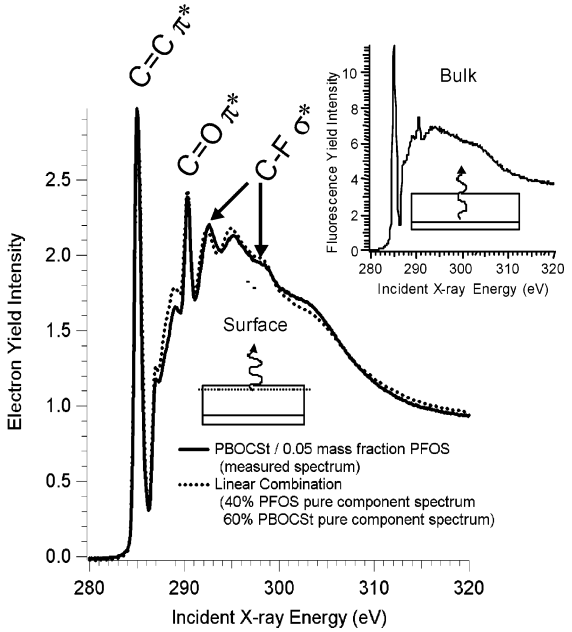

Figure 4. An appropriate linear combination of the pure component electron yield (surface) spectra from PFOS and PBOCSt (dotted line) is used to match the measured electron yield spectrum for PBOCSt/PFOS films. The inset shows the fluorescence yield (bulk) spectrum for the sample. While the fluorine peaks are strongly observed in the electron yield spectrum, they are not present in the fluorescence yield spectrum.

visible as well as the π^* transition associated with the carbonyl [C 1s $\rightarrow \pi^*_{C=O}$] on PBOCSt (290.3 eV) and the carbon−carbon double bonds [C 1s $\rightarrow \pi^*_{C=C}$] on the ring (285.0 eV). Using the pure component electron yield spectra from Figure 3, the measured electron yield spectra for the PBOCSt/PFOS film (solid line) in Figure 4 can be adequately fit with a linear combination (dotted line) of 0.4 times the pure PFOS spectrum and 0.6 times the pure PBOCSt spectrum. The inset shows the fluorescence yield (bulk) spectrum for the PBOCSt/PFOS sample. The carbon−fluorine σ^* peaks [C 1s $\rightarrow \sigma^*_{C-F}$] associated with the PFOS were not detected in the fluorescence yield spectrum, indicating a lower PFOS concentration in the bulk film relative to the film surface. The peaks in the fluorescence yield spectra appear blunted relative to the electron yield spectra. This is particularly obvious with the [C 1s $\rightarrow \pi^*_{C=O}$] on PBOCSt (290.3 eV). The blunted peaks are due to the fact that the incident X-ray excitation is not penetrating the entire film thickness. With strongly absorbing transitions, the penetration depth of the incident radiation decreases and the resulting fluorescence yield is lower than expected. Because the effective fluorescence yield sampling depth of strongly absorbing transitions is less than the sampling depth in weaker absorbing regions, the fluorescence yield peaks in the strongly absorbing regions become attenuated. The carbon−fluorine σ^* peaks [C 1s $\rightarrow \sigma^*_{C-F}$] associated with the PFOS would also be attenuated in the fluorescence yield spectra shown in the inset in Figure 4. However, these peaks are not just attenuated, they are completely absent. The absence of these peaks in the fluorescence yield spectrum and the presence of these peaks in the electron yield spectrum qualitatively verified that the bulk PFOS concentration is lower than the surface concentration.

A lack of the carbon−fluorine σ^* peaks [C 1s $\rightarrow \sigma^*_{C-F}$] associated with PFOS in the fluorescence yield spectrum in Figure 4 does not indicate that no PFOS is present in the bulk film. In fact, fluorescence yield measurements

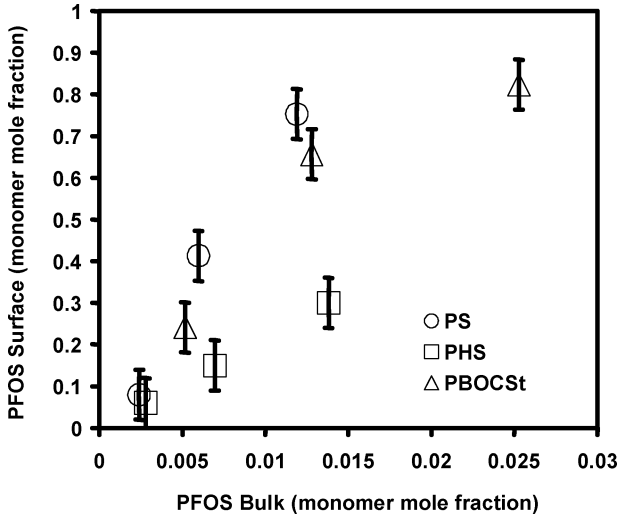

Figure 5. PFOS surface monomer mole fraction (measured by NEXAFS electron yield spectra) plotted against the bulk monomer mole fraction in a variety of polymers. Mole fraction is given in moles of PFOS per mole of polymer monomers.

over the fluorine K-edge absorption region clearly indicated the presence of PFOS in similar bulk films.[28] A PBOCSt/PFOS mixture with 0.05 PFOS mass fraction corresponds to a PFOS mole fraction of 0.013 relative to the moles of PBOCSt monomers. The linear spectral combination (shown in Figure 4) can be used to extract the surface monomer mole fraction of PFOS, but must be corrected to account for the carbon density in the PFOS molecules relative to the PBOCSt monomers. This relative carbon density was estimated from the ratio of the carbon edge jump of PBOCSt relative to PFOS in the pre-edge jump normalized spectrum for the neat components. For example, the edge-jump intensity (I_j defined in Figure 2 in arbitrary units) for PBOCSt was 1.17 and for PFOS was 0.41. The linear combination in Figure 4 gives 0.4/0.6 as the ratio of carbon signal from PFOS relative to carbon signal from PBOCSt. Converting the linear combination to a monomer mole fraction ratio requires normalizing with the carbon content in PBOCSt relative to PFOS (1.17/0.41). This conversion gives a value of (0.4/0.6)(1.17/0.41) = 1.9 for the moles of PFOS per mole of PBOCSt monomers, yielding a PFOS surface mole fraction of 0.65 = 1.9/(1.9 + 1). The primary uncertainty associated with measuring the PFOS surface monomer mole fraction is due to fitting the measured spectra for the polymer/PFOS films by a linear combination of the pure component spectra. The linear combinations provided an adequate fit with a relative standard uncertainty of ±0.05 for the fraction of each pure component spectra used. After converting this range of linear combinations to a monomer mole fraction, this translated to a relative uncertainty in the surface PFOS mole fraction ranging from 0.04 to 0.07.

Figure 5 plots the surface monomer mole fraction of PFOS (calculated from the NEXAFS electron yield spectra via the linear combination described in Figure 4) versus the bulk PFOS monomer mole fraction (calculated from mass measurements in the spin casting formulation). The monomer mole fractions are given in moles of PFOS per mole of polymer monomers. For PBOCSt, PHS, and PS, the surface monomer mole fraction of PFOS is much larger than the bulk. However, the amount of surface segregation is polymer dependent, with larger surface segregation of

(28) Lenhart, J. L.; Jones, R. L.; Lin, E. K.; Soles, C. L.; Wu, W.-L.; Fischer, D. A.; Sambasivan, S.; Goldfarb, D. L.; Angelopoulos, M. *J. Vac. Sci. Technol., B* **2002**, *20*, 2920.

PFOS in the nonpolar PBOCSt and PS polymers. With PS and PBOCSt, the surface monomer mole fraction of PFOS is 50−70 times the bulk fraction. With PHS, the surface monomer mole fraction is approximately 20 times the bulk value. The error bars in Figure 5 represent the relative standard uncertainty in the surface monomer mole fraction. The inset in Figure 4 shows the fluorescence yield carbon K-edge spectrum for the PBOCSt/PFOS film. Carbon−fluorine peaks are observed in the carbon K-edge electron yield spectrum but not observed in the carbon K-edge fluorescence yield spectrum, qualitatively verifying the PFOS surface enrichment. If the surface PFOS content were similar to the bulk value (0.05 mass fraction or 0.013 mole fraction), the carbon−fluorine σ^* peaks [C 1s → σ^*_{C-F}] would not be observed in the carbon edge electron yield spectra because the carbon−fluorine contribution from PFOS would be dominated by a large carbon background from the PBOCSt fraction. The fact that the carbon−fluorine peaks can be observed strongly in the carbon edge electron yield spectrum qualitatively illustrates a significant PFOS segregation to the film surface. The carbon−fluorine σ^* peaks [C 1s → σ^*_{C-F}] were also observed in the carbon edge electron yield spectra but not in the fluorescence yield spectra for PHS/PFOS and PS/PFOS films.

Surface segregation in polymers has been studied extensively. For polymeric systems, both entropic and enthalpic factors must be considered to determine surface compositions. For example, when similar interactions are present in the polymeric systems, entropic forces can drive chain ends,[29] lower molecular weight components,[30] and branched species[31] to preferentially segregate to a surface. Enthalpic interactions can also dictate surface composition. For end functionalized polymers and copolymers (block, graft, and random), the low surface energy functional group will concentrate at the polymer−air interface,[32−35] although entropic considerations associated with chain connectivity can limit the surface concentration of the functional group when compared to polymer blends. Near the polymer−substrate interface, the interaction between the functional group and the substrate can also impact segregation. For example, with diblock copolymers of polystyrene (PS) and poly(methyl methacrylate) (PMMA) on a silicone oxide substrate, the PMMA contacts the substrate while the PS contacts the air interface.[36] This is explained by a strong interaction between the PMMA and silicone oxide surface, and the low surface energy PS segments. In a similar copolymer system, if the silicon oxide surface is replaced by gold, the PS segments segregate to both the air and the gold interface,[37] possibly due to a specific interaction between the PS and gold. While structural considerations can influence surface composition of small molecule additives in polymers, enthalpic considerations dominate and low energy species such as fluorinated or siloxane additives can segregate extensively to the polymer−air interface.[38−40]

The driving force for surface segregation is the difference in the interfacial tensions of the small molecule and the polymer.[32] Therefore, it is interesting that the fluorinated PFOS exhibits more surface segregation in the nonpolar polymers (PS and PBOCSt) than in the polar polymer PHS, as one might expect more surface segregation of a fluorinated component to the higher energy surface of a polar polymer. However, PFOS is also an ionic species (see structure in Figure 3), and the ionic character of the PFOS is counterbalancing some of the effect of the fluorinated groups. It is possible that a competition exists between the drive to lower the surface energy by segregation of fluorinated groups to the air interface, and strong ionic−dipole interactions between the PFOS and the polar polymer in the bulk of the film. With a nonpolar polymer, the surface energy effect dominates, leading to high concentrations of PFOS at the interface. With the polar polymer, the ionic−dipolar interactions between PHS and PFOS in the bulk film become important, leading to less surface segregation. To test this hypothesis, we are currently investigating the influence of different types of PAGs, including nonionic PAGs, on surface segregation.

Figure 6 compares the electron and fluorescence yield for the PBOCSt/PFOS films after various photolithography processing conditions. By monitoring the C=O π^* transition [C 1s → $\pi^*_{C=O}$] from the carbonyl on PBOCSt, the extent of deprotection can be followed during processing (see deprotection reaction schematic in Figure 1). In Figure 6, the spectra are both pre-edge and post-edge jump normalized. The post-edge jump normalization involves dividing the pre-edge jump normalized spectra by the edge jump intensity (I_j from Figure 2). This eliminates the spectral dependence on total carbon content in the sampling volume; thus changes in the NEXAFS peak intensity are due to chemical changes in the system. The films in Figure 6 were treated with typical resist processing conditions, including post-apply bake (PAB) for 60 s at 100 °C; UV exposure 500 mJ/cm^2 from a broadband source 220 nm to 260 nm; and post-exposure bake (PEB) at 100 °C for various times. Figure 6a shows the fluorescence yield (bulk) spectra from the samples. A strong carbonyl peak is present in the PAB and PAB/UV treated samples, which overlap each other. After a 20 s PEB at 100 °C, the peak at 290.3 eV decreases by approximately $^1/_2$. After 2 min PEB, the peak at 290.3 eV decreases further, indicating that the bulk of the resist film is not completely deprotected after the 20 s PEB. The sampling depth of the fluorescence yield is dictated by the incident X-ray energy and the angle of the incident radiation. Over the carbon K-edge region, the sampling depth is approximately 100−200 nm. These films were approximately 300 nm thick, so the fluorescence yield is probing roughly one-half the film thickness. The UV exposure utilized to convert PFOS to an acidic species is from a broad source between 220 and 260 nm. Over this wavelength range, the UV radiation penetrates the entire film thickness. In fact, PBOCSt-based resist polymers are utilized with 248 nm exposure tools, with typical resist film thickness greater than 500 nm. The PBOCSt polymer was chosen for lithographic patterning with 248 nm radiation in part due to effective transparency at this wavelength. Therefore, the fluorescence yield spectra in Figure 6a are representative of the bulk chemistry in the films after UV exposure.

Figure 6b shows the electron yield (surface) spectra for the same PBOCSt/PFOS films. After both the PAB and a PAB + UV, the C=O π^* transition [C 1s → $\pi^*_{C=O}$] at

(29) Theodorou, D. N. *Macromolecules* **1989**, *22*, 4578.
(30) Hariharan, A.; Kumar, S. K.; Russell, T. P. *Macromolecules* **1990**, *23*, 3584.
(31) Walton, D. G.; Mayes, A. M. *Phys. Rev. E* **1996**, *54*, 2811.
(32) Koberstein, J. T. *J. Polym. Sci., Part B: Polym. Phys.* **2004**, *42*, 2942.
(33) Hwang, S. S.; Ober, C. K.; Perutz, S.; Iyengar, D. R.; Schneggenburger, L. A.; Kramer, E. J. *Polymer* **1995**, *36*, 1321.
(34) Jannasch, P. *Macromolecules* **1998**, *31*, 1341.
(35) Hopken, J.; Moller, M. *Macromolecules* **1992**, *25*, 1461.
(36) Anastasiadis, S. H.; Russell, T. P.; Satija, S. K.; Majkrzak, C. F. *J. Chem. Phys.* **1990**, *92*, 5677.
(37) Russell, T. P.; Coulon, G.; Deline, V. R.; Miller, D. C. *Macromolecules* **1989**, *22*, 4600.
(38) Gorelova, M. M.; Pertsin, A. J.; Volkov, I. O.; Filimonova, L. F.; Makarova, L. I.; Zhdanov, A. A. *J. Appl. Polym. Sci.* **1995**, *57*, 227.
(39) Ebbens, S. J.; Badyal, J. P. S. *Langmuir* **2001**, *17*, 4050.
(40) Walters, K. B.; Schwark, D. W.; Hirt, D. E. *Langmuir* **2003**, *19*, 5851.

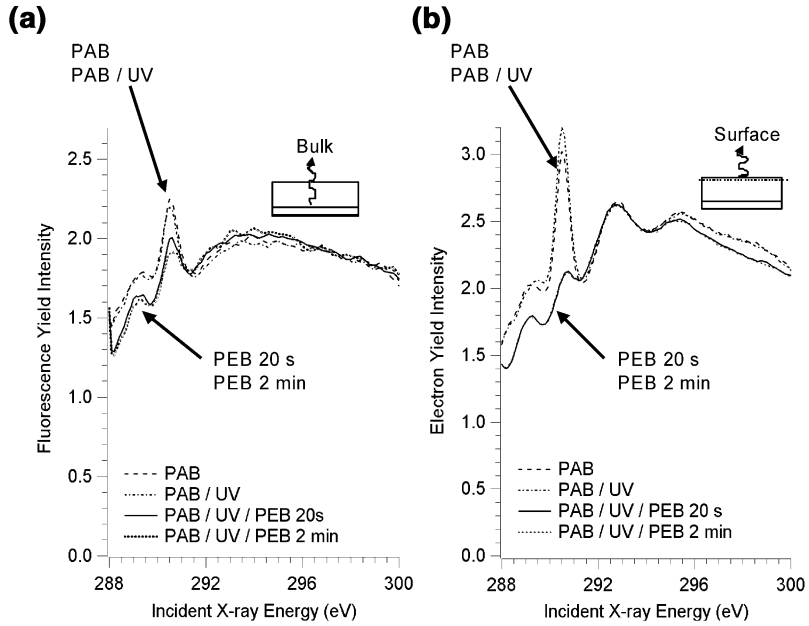

Figure 6. (a) The fluorescence yield spectrum (bulk) is shown for the PBOCSt/PFOS films after different processing steps. (b) The electron yield spectrum (surface) is shown for the same PBOCSt/PFOS films. Comparison of the electron and fluorescence yield shows that the surface reaction rate is faster than the bulk.

290.3 eV is large in the electron yield (Figure 6b), indicating the polymer is still protected. However, after a short 20 s PEB at 100 °C, the carbonyl peak completely disappears in the electron yield, indicating complete deprotection at the film surface. Also shown in Figure 6b is the curve for the PBOCSt/PFOS film after 2 min PEB. This curve overlaps with the PBOCSt/PFOS film after the 20 s PEB in the carbonyl region near 290.3 eV, verifying that complete surface deprotection occurs in the first 20 s of post-exposure baking. Comparison of the electron yield with the fluorescence yield spectrum illustrates that the surface reaction rate is faster than the bulk. In addition, the electron yield spectra exhibit strong carbon−fluorine peaks between 292 and 298 eV from the PFOS. Because these peaks are not observed in the fluorescence yield spectra, this further illustrates significant PFOS segregation to the film surface. This large surface segregation of the PAG would lead to a higher acid content near the air interface and increase the deprotection reaction rate.

As was mentioned earlier with the discussion of Figure 4, the peaks in the fluorescence yield spectra appear blunted relative to the electron yield spectra due to attenuation of the X-ray excitation and the resulting decrease in fluorescence yield sampling depth, while blunting of the carbonyl absorption region in Figure 6a makes quantitative interpretation of the bulk deprotection rate difficult. The qualitative observation that the deprotection reaction in the bulk film is not completed after the 20 s PEB is still valid, indicating that the surface deprotection is occurring faster than the bulk.

In Figure 6, there were no delay times between successive processing steps: spin coat, PAB, UV exposure, PEB. However, time delays between the various steps can have a significant impact on the resultant lithographic patterns. Figure 7 shows the carbon K-edge fluorescence (Figure 7a) and electron yield (Figure 7b) spectra for a PBOCSt/PFOS film after the PAB only, and after a PAB + UV + PEB sequence. The NEXAFS spectra in Figure 7a,b are from the same sample. However, for this sample, a 10 min delay time was incorporated between the UV exposure and PEB; this is called a post-exposure delay (PED). In the carbon edge fluorescence yield spectra, a

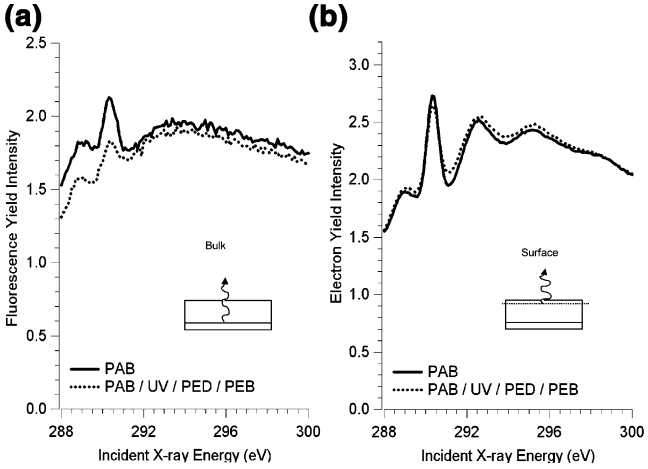

Figure 7. The carbon K-edge fluorescence yield spectra (a) and carbon K-edge electron yield spectra (b) are shown for the PBOCSt/PFOS film after PAB (−), UV exposure, a 10 min PED, and a 2 min post-exposure bake at 100 °C (· · · ·).

carbonyl peak at 290.3 eV is observed in the PAB film. After UV exposure, 10 min PED, and a 2 min PEB at 100 °C, the peak area has dramatically decreased, indicating deprotection in the bulk of the resist film (Figure 7a). In the carbon edge electron yield spectra, the peak decreases only slightly after UV exposure and PEB, indicating incomplete deprotection at the film surface (Figure 7b).

The mechanisms leading to the incomplete surface deprotection reaction due to PED have not been determined and are a focus of our current research. A likely explanation is acid neutralization in the resist film due to atmospheric contaminants. Nalamasu et al. showed that the PED time was critical to the performance of chemically amplified resists.[14] A PED of several minutes led to an aqueous-base insoluble residue at the resist/air interface, while longer PEDs prevent the lithographic image from being developed. It was shown that resist performance deteriorated dramatically in basic environments, but could be improved by controlling the processing atmosphere or coating the resist with a base-neutralizing (weakly acidic) polymer layer. Incomplete deprotection

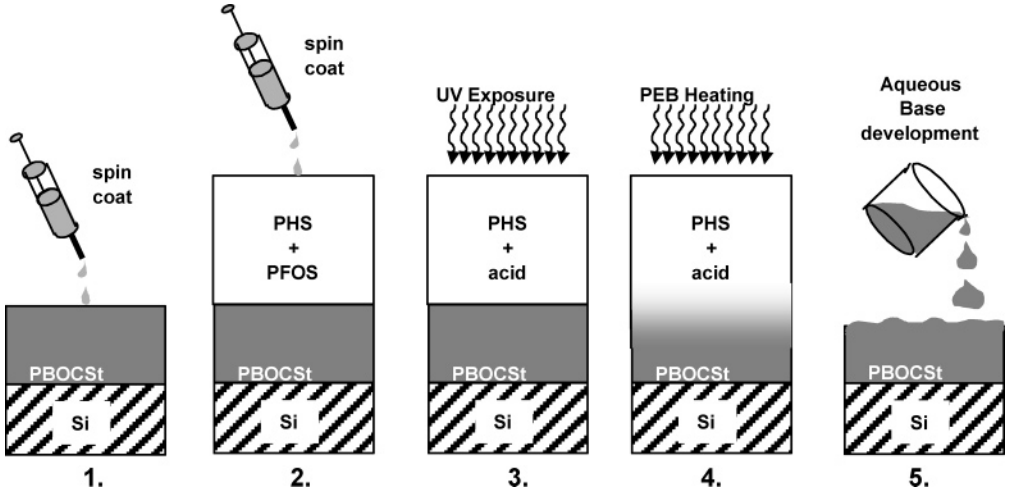

Figure 8. A schematic of the experiments used to generate a model line edge region. NEXAFS depth profiling was conducted on the developed bilayer sample, stage 5 from above.

near the resist/air interface was suggested as the cause of the insoluble residual layer. MacDonald et al. also showed that airborne amine contaminants degrade resist performance by leading to the formulation of a thin insoluble skin at the resist/air interface.[15] Hinsberg et al. illustrated that the extent of base contamination in a resist film depends on the polymer solubility parameter, and the temperature difference between the PAB and the polymer glass transition.[16] The extent of resist contamination will depend on the polymer−contaminant interaction as well as the physical and thermal properties of the resist films.

PED is considered to be a critical factor in t-topping.[12,14] These experiments illustrate that a PED of 10 min can lead to incomplete surface deprotection, explaining the insoluble skin in t-topped or closed resist patterns with PED incorporated in the processing. The PAB temperature of 100 °C for these PBOCSt/PFOS films was below the glass transition of bulk PBOCSt ($T_g \approx 130$ °C). By comparison to the work of Hinsberg et al.,[16] this would lead to an uptake of atmospheric contaminants by the resist film, because more contaminant absorbs in resists with PAB temperatures well below the bulk polymer T_g. In addition, the incomplete surface deprotection was observed in these PBOCSt/PFOS films despite having significant excess PFOS at the film surface. Apparently, atmospheric contamination can still neutralize the excess surface acidity. Qualitatively, we observed that short PED (<15 min) led to surface quenching of the deprotection, while the bulk reaction still proceeded. For longer PED times (>15 min), both the surface and the bulk reaction were quenched as no significant decrease in the carbonyl peak in either the electron or the fluorescence yield spectra was observed for these longer times. This is consistent with a process involving contaminant absorption on the film surface and gradual diffusion of the contaminant into the bulk of the film.

4.2. Surface Depth Profiling with NEXAFS. The electron yield signal in NEXAFS is surface sensitive. By adjusting a negative voltage bias on the electron yield detector, different effective surface sampling depths can be probed. When the polymer film is excited by the incident X-ray radiation, the entire region of the film that absorbs photons also emits electrons. Only the electrons emitted near the top 1−10 nm from the film surface have enough energy to escape the surface potential. The electron yield detector has a grid where a negative voltage bias can be placed across the grid. The electrons that escape the surface potential of the film, but were emitted from furthest within the film, will be low in energy due to inelastic interactions with other atoms. These low energy electrons will not have enough kinetic energy to pass the negative detector bias. If the negative detector bias is gradually increased, progressively higher energy electrons are detected, and the effective electron yield sampling depth is closer to the film surface. This depth profiling technique has been utilized to study self-assembled monolayers[41] and relaxation of thin polymer films,[42] and typical electron mean free paths (effective probing depths) can be varied from approximately 10 to 50 Å by adjusting the retarding voltage on the electron yield detector.[43]

We take advantage of this surface depth profiling capability to study the chemical composition profile of a model developed line edge region. For these experiments, bilayer samples of PBOCSt and PHS were spun cast onto silicon wafers as discussed briefly in the Experimental Section and in detail elsewhere.[44,45] A schematic of these bilayer samples is shown in Figure 8. The wafers were cleaned by immersion in sulfuric acid and hydrogen peroxide solution followed by a rinse in deionized water. A hydrophobic surface was generated by treating the wafers with hexamethyldisilazane (HMDS) vapor in a vacuum oven. The bottom PBOCSt layer was spun cast from solution with PGMEA and soft baked for 60 s at 130 °C. A top layer of PHS (with a 5% mass loading of PFOS) was spun cast on PBOCSt from a solution of *n*-butanol. The samples were exposed to UV radiation, generating acid in the PHS feeder layer, and post-exposure baked for various times at 90 °C. During PEB, the acid diffuses into the PBOCSt underlayer and initiates a diffusion/deprotection front that propagates into the underlayer. After PEB, the soluble top portion of the bilayer film was removed (developed) by immersion in aqueous 0.26 N tetra-methylammonium-hydroxide (TMAH) solution, leaving a residual deprotection profile in the final developed underlayer. NEXAFS measurements were then conducted

(41) Genzer, J.; Kramer, E. J.; Fischer, D. A. *J. Appl. Phys.* **2002**, *92*, 7070.
(42) Liu, Y.; Russell, T. P.; Samant, M. G.; Stohr, J.; Brown, H. R.; Cossy-Farvre, A.; Diaz, J. *Macromolecules* **1997**, *30*, 7768.
(43) Zharnikov, M.; Frey, S.; Heister, K.; Grunze, M. *J. Electron Spectrosc. Relat. Phenom.* **2002**, *124*, 15.
(44) Goldfarb, D. L.; Angelopoulos, M.; Lin, E. K.; Jones, R. L.; Soles, C. L.; Lenhart, J. L.; Wu, W. L. *J. Vac. Sci. Technol., B* **2001**, *19*, 2699.
(45) Lin, E. K.; Soles, C. L.; Goldfarb, D. L.; Trinque, B. C.; Burns, S. D.; Jones, R. L.; Lenhart, J. L.; Angeloupolos, M.; Willson, C. G.; Satija, S. K.; Wu, W. L. *Science* **2002**, *297*, 372.

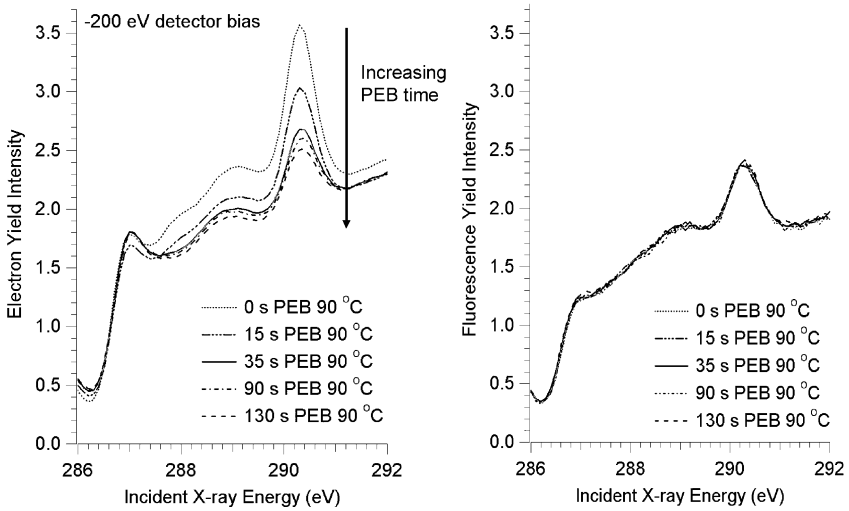

Figure 9. (Left) NEXAFS carbon edge electron yield spectra at a constant detector bias of −200 eV are shown for the developed bilayer samples with different PEB times at 90 °C. (Right) The fluorescence yield spectra are shown for the same bilayer samples. The fluorescence yield was measured simultaneously with the electron yield.

on the developed bilayer samples (step number 5 in Figure 8) as a function of the electron yield detector bias. To understand the physics of the dissolution process and the potential link between line edge composition and the pattern shape, size, and roughness, it is important to develop techniques to measure the composition profile of the line edge region. We start by utilizing NEXAFS surface depth profiling on the model bilayer interfacial regions.

Figure 9 shows NEXAFS pre-edge and post-edge jump normalized spectra in the carbonyl absorption region, between 288 and 292 eV, for the bilayer samples after various PEB times at 90 °C and development in TMAH solution. For these NEXAFS spectra, the electron yield detector bias was fixed at −200 eV (sampling depth of roughly 3 nm, or three monomeric layers). Because the electron density values of both PHS and PBOCSt are similar, fixing the detector bias essentially fixes the surface sampling volume. The top spectrum is for the PBOCSt/PHS bilayer without a PEB and after development in TMAH. In this sample, no deprotection occurs in the PBOCSt underlayer, and the carbonyl absorption is large. However, the carbonyl absorption clearly decreases with increasing bake times, indicating that the extent of deprotection in the surface sampling volume is increasing. The surface composition of the developed bilayer is changing with increasing PEB times. One possible explanation is that the PBOCSt composition at the film/air interface remains constant, while the PBOCSt composition profile broadens into the film due to a progression of the diffusion/reaction profile at short times. Another possible explanation is that the actual PBOCSt composition at the film/air interface is decreasing with increasing bake times. The right side in Figure 9 shows the fluorescence yield spectra for each of these bilayers at various PEB times. The fluorescence yield spectra were independent of the PEB time, indicating that the bulk composition of the film remains unchanged. Because the fluorescence yield is collected from 100 to 200 nm into the film, the fact that the fluorescence signal does not change with PEB time indicates that the compositional change observed in the electron yield spectra is localized very close to the film/air interface.

Figure 10 shows the NEXAFS spectra as a function of detector bias for a bilayer sample that was subjected to a short 15 s PEB at 90 °C. The spectra are both pre- and post-edge jump normalized so the carbonyl peak area

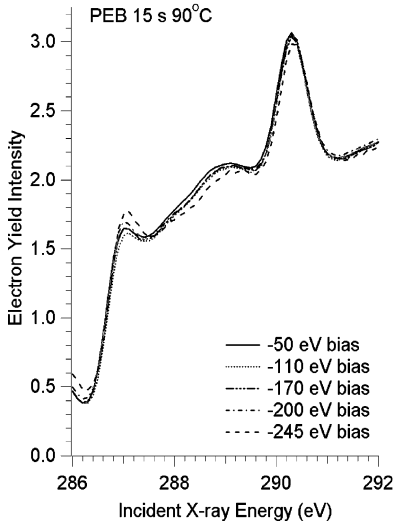

Figure 10. NEXAFS carbon edge electron yield spectra are shown as a function of detector bias for a bilayer with a 15 s PEB at 90 °C. The area of the carbonyl absorption does not change significantly with detector bias.

represents the carbonyl group fraction in the sampling volume. As the negative detector bias increases, the effective electron yield sampling depth is progressively closer to the film surface. The carbonyl peak area for this short PEB sample does not change significantly with detector bias. This means that the composition does not change with the surface depth sampling volume and indicates a diffuse surface composition profile over the total sampling volumes scanned with the various detector bias settings.

Figure 11 shows the NEXAFS spectra as a function of detector bias for a bilayer sample that was subjected to a 60 s PEB at 90 °C. Again, the spectra are both pre- and post-edge jump normalized. In contrast to the 15 s PEB, with the 60 s PEB the carbonyl peak area decreases with increasing detector bias. Again, because the sampling area in the electron yield is progressively closer to the film surface with increasing detector bias, a decrease in the carbonyl peak area with increasing bias indicates a change in the surface composition and a composition change over the sampling volumes scanned with the differing bias settings. A comparison of the bias dependence of the

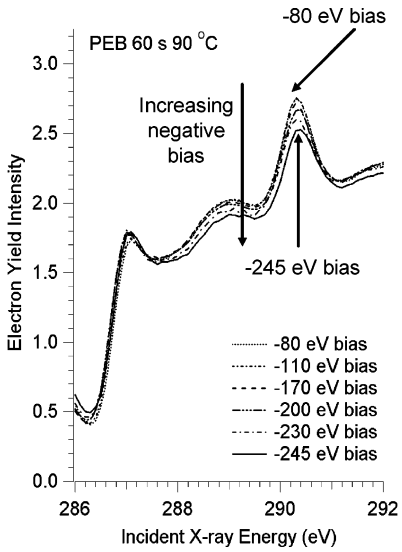

Figure 11. NEXAFS carbon edge electron yield spectra are shown as a function of detector bias for a bilayer with a 60 s PEB at 90 °C. The area of the carbonyl absorption decreases with increasing negative bias.

carbonyl peak areas at 15 s (Figure 10) and 60 s (Figure 11) PEB times illustrates a change in the surface composition profile after development with increasing bake times. First, Figure 10 shows that the carbonyl peak has no bias dependence and indicates a diffuse surface composition profile, while in Figure 11 the carbonyl peak shows a subtle bias dependence, indicating a less diffuse profile. Second, a qualitative comparison of the carbonyl peak area (288−292 eV) shows that for the short PEB (15 s at 90 °C) the peak areas are larger than for the longer PEB time (60 s at 90 °C). These data illustrate that the surface PBOCSt fraction (at the resist−air interface) is larger for the short bake times. While the surface composition profile changes with time, it is unclear how the breadth of the buried reaction/diffusion profile (before development) influences the corresponding dissolution process and the resulting surface composition profile and line edge roughness. While these areas are currently under investigation by a number of research groups, the application of high-resolution measurement capabilities allows the potential to make these connections. We are currently developing a theoretical formalism to quantitatively extract the surface composition profile from the NEXAFS bias-dependent spectra.

5. Conclusions

Exploiting the chemical and surface sensitivity of NEXAFS proved useful for probing critical interfacial problems in photoresist films. First, segregation of a photoacid generator was observed at the resist−air interface. This surface segregation led to a higher acid content and faster deprotection reaction at the interface relative to the bulk of the film. NEXAFS also indicated that a post-exposure delay slowed the deprotection reaction at the resist−air interface, presumably due to absorption of atmospheric contaminants on the film surface. The impact of the post-exposure delay was important despite the enhanced surface concentration of the photo acid generator. Second, a NEXAFS surface depth profiling technique was applied to a model resist line edge region. The depth profiling illustrated that the surface composition of a line edge region is not constant at the assumed solubility switch of the resist, but dependent on the post-exposure bake time. The depth profiling technique has potential to help extract surface compositional gradients from patterned surfaces.

Acknowledgment. Sandia is a multiprogram laboratory operated by Sandia Corp., a Lockheed Martin Co., for the United States Department of Energy under contract DE-AC04-94AL85000. The resist research involved collaboration between the National Institute of Standards and Technology and IBM and was supported by the Defense Advanced Research Projects Agency under grant N66001-00-C-8083.

LA047160Z